Available online at www.sciencedirect.com
SCIENCE DIRECT®
Journal of Computational Physics 210 (2005) 656–675
JOURNAL OF COMPUTATIONAL PHYSICS
www.elsevier.com/locate/jcp

Numerical methods for multiscale transport equations and application to two-phase porous media flow

Xingye Yue [a,*], Weinan E [b]

[a] Department of Mathematics, Suzhou University, No. 1 Shizi Street, Suzhou 215006, China
[b] Department of Mathematics and PACM, Princeton University, NJ 08544, USA

Received 11 October 2004; received in revised form 28 April 2005; accepted 2 May 2005
Available online 14 July 2005

Abstract

We discuss numerical methods for linear and nonlinear transport equations with multiscale velocity fields. These methods are themselves multiscaled in nature in the sense that they use macro and micro grids, multiscale test functions. We demonstrate the efficiency of these methods and apply them to two-phase flow in heterogeneous porous media.

Keywords: Multiscale transport equation; Two-phase flow in porous media; Numerical methods

1. Introduction

The purpose of this paper is to construct efficient numerical methods for transport equations of the type

$$u_t^\varepsilon + \nabla \cdot (a^\varepsilon(x) f(u^\varepsilon)) = 0 \tag{1.1}$$

with an initial condition $u^\varepsilon(x,0) = u_0^\varepsilon$. Here, $a^\varepsilon(x)$ is some velocity field that varies on multiple length scales, the simplest example being

$$a^\varepsilon(x) = a\left(x, \frac{x}{\varepsilon}\right), \tag{1.2}$$

where $a(x,y)$ is a smooth vector-valued function of x and y, which is periodic in y with period $I = [0,1]^d$. Later on we will also study the case when $a(x,y)$ is random in y. Our primary motivation comes from porous medium flows where the multiscaled nature of the velocity field is a consequence of the multiple scales

* Corresponding author.
E-mail addresses: xyyue@suda.edu.cn (X. Yue), weinan@math.princeton.edu (W. E).

0021-9991/$ - see front matter
doi:10.1016/j.jcp.2005.05.009

in the properties of the medium such as porosity and permeability. For example, in Buckley–Leverett equation, f is the fractional flow: $f(u) = [v_w/(v_o + v_w)]$, where $v_o = v_o(u)$ and $v_w = v_w(u)$ are the velocity of the oil and water phases.

In principle we should also include diffusive terms in the saturation equations. There are three distinguished limits when both advection and diffusion terms are present. The first is when diffusion is dominant at the small scale. The second is when diffusion and advection balance each other at the small scale. The last is when advection is dominant at the small scale. The last case is the most difficult one, since in this case the macroscale behavior exhibits memory effects, as we discuss below. In contrast, the macroscale behavior is much more local in the first and second cases, and standard ideas such as the heterogeneous multiscale method (HMM) applies. Therefore we will focus in this paper on the last case. In this situation the diffusion term does not play any significant role, and hence we will neglect it for simplicity.

Various attempts have been made to design efficient numerical methods for problems of the type (1.1). So far there has not been any general method that truly exploits the multiscaled nature of the problem. Most numerical work in this area are either based on empirical closure or upscaling methods (see [3,8,9,12,20]), or restricted to rather special flow fields (velocity fields). The difficulty is mainly due to the fact that the effective behavior of the tracer field u^ε at large scales is rather complicated and may depend on past history. As a result, general multiscale methods such as the heterogeneous multiscale method (HMM) which has been successful for a large class of problems, does not work directly for the present problem (for a discussion on this, see [5]).

Our basic assumption is that the microscopic behavior changes smoothly (in a statistical sense) over the macroscale. Such a behavior can be efficiently probed using multiscale test functions. One can think of this in the following way. At each macroscopic grid point, we do not just carry the function value at that particular grid point, but rather the complete information on the local microstructure (see Fig. 1). Such ideas have been used analytically in the work of Nguetseng [15], E [4], Evans [11] and Allaire [1], and in the numerical work of Schwab et al. [13,17]. But our work involves considerable extension.

In the following of the paper, we first discuss the homogenization results for linear multiscale transport problems in Section 2. We present two numerical methods in Section 3 and some numerical results in Section 4. In Section 5, we discuss two extensions for nonlinear transport problems and for problems with random velocity fields. Then in Section 6, we apply the method developed in Section 5 to two-phase flow in heterogeneous porous media. Finally in Section 7, we draw some conclusions.

2. Homogenization results

To better appreciate the complexity of the behavior of the solutions of (1.1), we first summarize the variety of homogenization results for the simplest case when the microstructure in the velocity field a^ε is periodic and the flux is linear. We will also assume that $a(x, y)$ is incompressible

$$\nabla_x \cdot a(x, y) = 0, \quad \nabla_y \cdot a(x, y) = 0. \tag{2.1}$$

There are two types of homogenization results concerning (1.1). The first type aims at deriving homogenized equations for the local averages of u^ε, neglecting information on the microscale details. The second type of results captures the local microscale details and represents them by introducing additional variables.

2.1. Effective equations for averaged quantities

We will deal with the two-dimensional case. The results summarized below might be special to two dimensions.

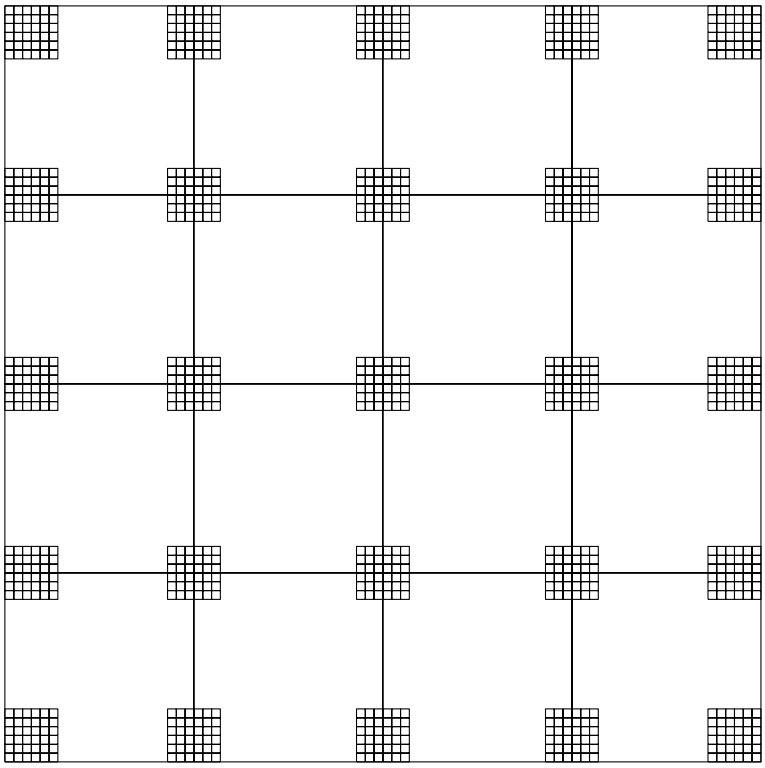

Fig. 1. Illustration of the methodology. At each macroscale grid point in physical (x-) space, not only the function value at that point, but the local microstructure is computed. The fine grid can be thought of as being in the y-space, the additional variables we use to represent the microstructure, as we discuss below in Section 2. The size of the cells where fine grid computation is carried out is a few times of the local correlation length of the microstructure for random velocity field, and is right a period for periodic velocity field.

Let us assume that $a^\varepsilon(x) = (a_1(\frac{x}{\varepsilon}), a_2(\frac{x}{\varepsilon}))$ and

$$a(y) = (a_1(y), a_2(y)) = \left(-\frac{\partial\varphi}{\partial y_2}, \frac{\partial\varphi}{\partial y_1}\right),$$

φ is the stream-function associated with the velocity field a.

1. *Ergodic velocity fields.* Let

$$\bar{a}_1 = \int_{[0,1]^2} a_1(y)\mathrm{d}y, \quad \bar{a}_2 = \int_{[0,1]^2} a_2(y)\mathrm{d}y.$$

Assume that $\bar{a}_1$ and $\bar{a}_2$ are incommensurate and that the velocity field a has no singular points, i.e. $a_1^2(y) + a_2^2(y) > 0$ for all $y \in [0,1]^2$, then it can be easily shown [4] that the solutions of

$$u_t^\varepsilon + \nabla_x \cdot (a^\varepsilon(x)u^\varepsilon) = 0$$

have the form

$$u^\varepsilon(x,t) = \bar{u}(x,t) + \mathrm{o}(1),$$

where $\bar{u}$ satisfies the equation

$$\bar{u}_t + \nabla_x \cdot (\bar{a}\bar{u}) = 0$$

with $\bar{a} = (\bar{a}_1, \bar{a}_2)$.

2. *Cellular flows.* Consider the case when $\varphi(y) = \sin 2\pi y_1 \sin 2\pi y_2$. The streamlines of a are all closed except the separatrices. It is easy to see that in this case [4]

$$\bar{u}(x,t) = \lim_{\varepsilon \to 0} u^\varepsilon(x,t) = u_0(x).$$

In other words, the leading order term of u^ε satisfies the equation

$$\bar{u}_t = 0.$$

3. *Shear flows.* Let $a(y) = (a_1(y_2), 0)$, where $a_1(y_2)$ is periodic in y_2 with period $[0,1]$. In this case, u^ε has the form

$$u^\varepsilon(x,t) = U\left(x_1, x_2, \frac{x_2}{\varepsilon}, t\right) + o(1),$$

where $U(x_1, x_2, y_2, t)$ is periodic in y_2 with period $[0,1]$. If we define

$$\bar{u}(x,t) = \int_{[0,1]} U(x_1, x_2, y_2, t) \mathrm{d}y_2,$$

then $\bar{u} = \bar{u}(x,t)$ satisfies [18]

$$\bar{u}_t + \bar{a}_1 \bar{u}_{x_1} = \frac{\partial^2}{\partial x_1^2} \int_{-\infty}^{\infty} \mathrm{d}\omega(\lambda) \int_0^t \bar{u}(x_1 + \lambda(t-s), x_2, s) \mathrm{d}s,$$

where $\mathrm{d}\omega(\lambda)$ is a measure determined by a_1.

This example illustrates the complexity of the dynamics of the locally averaged quantities $\bar{u}$: it is nonlocal and has memory effects. As a result, HMM type of methods are not directly applicable to such problems [5,6].

These three examples illustrate the complex variety of behavior that can occur, depending on the nature of the small scale velocity fields. It also shows that when designing the numerical methods, it is important to keep at some parts of the microscale information. This is the guideline that we will follow below.

2.2. Parameterizing the microstructure

An alternative homogenization approach is to introduce additional variables to parameterize the microscale behavior of the solutions. For the transport equations this was done in [4] using a result of Nguetseng [15]. Here we provide a less rigorous but more intuitive derivation.

The basic idea is to probe the multiscale behavior of u^ε using multiscale test functions. Writing (1.1) in a weak form (for linear case: $f(u) = u$)

$$\int_{\mathbb{R}^2 \times \mathbb{R}^+} (\varphi_t^\varepsilon u^\varepsilon + (\nabla_x \varphi^\varepsilon \cdot a^\varepsilon) u^\varepsilon) \mathrm{d}x \, \mathrm{d}t + \int_{\mathbb{R}^2} \varphi^\varepsilon(x,0) u^\varepsilon(x,0) \mathrm{d}x = 0$$

for all sufficiently smooth φ^ε with compact support in $\mathbb{R}^2 \times [0,\infty)$ and with the form $\varphi^\varepsilon(x,t) = \varphi(x, \frac{x}{\varepsilon}, t)$. Let us assume that u^ε has the form

$$u^\varepsilon(x,t) = U\left(x, \frac{x}{\varepsilon}, t\right) + o(1),$$

where $U(x,y,t)$ is periodic in y. Noticing that

$$\int_{\mathbb{R}^2 \times \mathbb{R}^+} U\left(x, \frac{x}{\varepsilon}, t\right) \varphi\left(x, \frac{x}{\varepsilon}, t\right) \mathrm{d}x \, \mathrm{d}t \to \int_{\mathbb{R}^2 \times [0,1]^2 \times \mathbb{R}^+} U(x,y,t) \varphi(x,y,t) \mathrm{d}x \, \mathrm{d}y \, \mathrm{d}t,$$

as $\varepsilon \to 0$, we obtain, to the leading order that

$$\int_{\mathbb{R}^2\times[0,1]^2\times\mathbb{R}^+} (\nabla_y\varphi(x,y,t)\cdot a(x,y))U(x,y,t)\mathrm{d}x\,\mathrm{d}y\,\mathrm{d}t = 0.$$

Since φ is arbitrary, we obtain

$$\nabla_y\cdot(a(x,y)U(x,y,t)) = 0 \tag{2.2}$$

in the sense of distribution.

Next we let $\varphi^\varepsilon(x,t) = \varphi(x,\frac{x}{\varepsilon},t)$, but φ satisfies

$$\nabla_y\cdot(a(x,y)\varphi(x,y,t)) = 0,$$

i.e. for fixed (x,t), φ is constant along the streamlines of a, we obtain

$$\int_{\mathbb{R}^2\times\mathbb{R}^+}\mathrm{d}x\,\mathrm{d}t\int_{[0,1]^2}(\varphi_t+\nabla_x\varphi\cdot a)U(x,y,t)\mathrm{d}y+\int_{\mathbb{R}^2}\mathrm{d}x\int_{[0,1]^2}\varphi(x,y,0)U_0(x,y)\mathrm{d}y = 0, \tag{2.3}$$

where $U_0(x,y)$ is the weak limit of $u_\varepsilon(x,0) = u_0^\varepsilon(x)$. This is the weak form of the homogenized equation for U. Denote by $\mathscr{H}$ the subspace of $L^2_{\mathrm{loc}}(\mathbb{R}^2\times\mathbb{R}^+\times[0,1]^2)$ that consists of functions φ satisfying (2.2), i.e.

$$\mathscr{H} = \left\{\varphi\in L^2_{\mathrm{loc}}(\mathbb{R}^2\times[0,1]^2\times\mathbb{R}^+):\ \nabla_y\cdot(a(x,y)\varphi(x,y,t)) = 0\right\}, \tag{2.4}$$

where the equation is valid in the sense of distribution. Let $\mathscr{P}$ be the L^2 projection operator to $\mathscr{H}$, i.e. for $w\in L^2_{\mathrm{loc}}(\mathbb{R}^2\times[0,1]^2\times\mathbb{R}^+)$, $\mathscr{P}w\in\mathscr{H}$ such that

$$\int_{\mathbb{R}^2\times[0,1]^2\times\mathbb{R}^+}\mathscr{P}wv\,\mathrm{d}x\,\mathrm{d}y\,\mathrm{d}t = \int_{\mathbb{R}^2\times[0,1]^2\times\mathbb{R}^+} wv\,\mathrm{d}x\,\mathrm{d}y\,\mathrm{d}t\quad\forall v\in\mathscr{H}.$$

Then we can reformulate the equations for U as

$$U\in\mathscr{H},\quad \mathscr{P}(U_t+\nabla_x\cdot(aU)) = 0 \tag{2.5}$$

with initial data $U(x,y,0) = U_0(x,y)$.

Or in an equivalent form as

$$U\in\mathscr{H},\quad U_t+\nabla_x\cdot(aU)\in\mathscr{H}^\perp \tag{2.6}$$

with initial data $U(x,y,0) = U_0(x,y)$.

It is useful to consider some special examples.

Example 1. The shear flow. In this case, the homogenized equation takes the form $U = U(x,y_2,t)$,

$$U_t + a_1(y_2)U_{x_1} = 0. \tag{2.7}$$

Note that in this form, the homogenized equation is quite simple and has no nonlocal and memory effects.

Example 2. Ergodic velocity fields. In this case $\mathscr{H}$ consists functions that are independent of y. Hence $U = U(x,t)$ and

$$U_t+\nabla_x\cdot(\bar{a}U) = 0.$$

Example 3. One-dimensional case. If we apply the same technique to the one-dimensional model

$$u^\varepsilon_t+(a^\varepsilon u^\varepsilon)_x = 0,$$

we then get the following system of homogenized equations for $U = U(x,y,t)$:

$$\partial_y(a(x,y)U) = 0,$$
$$\int_0^1 (U_t + (aU)_x)\mathrm{d}y = 0.$$

Assuming that $a(x,y) \neq 0$, we can write

$$U(x,y,t) = \frac{W(x,t)}{a(x,y)}.$$

Then we have

$$\int_0^1 \frac{W_t}{a(x,y)}\mathrm{d}y + \int_0^1 W_x \mathrm{d}y = 0.$$

Hence

$$W_t + \left(\int_0^1 \frac{1}{a(x,y)}\mathrm{d}y\right)^{-1} W_x = 0.$$

3. Numerical methods

Next we discuss how to solve (2.5) numerically. Even though (2.5) is only derived for the special case of periodic homogenization, the basic underlying idea, namely to evolve the local microstructure of u^ε instead of just values of u^ε at equally spaced grid points, is of general relevance. We will discuss this in Sections 5 and 6.

3.1. The penalty method

Regarding Eq. (2.2) as a constraint, we can deal with it by penalty method. First we define an energy functional $F(U)$ by

$$F(U) = \frac{1}{2}\int_Y |\, a \cdot \nabla_y U|^2 \mathrm{d}y$$

for $U \in G = \{U$ is periodic w.r.t $y \in Y = [0,1]^2$ and $a \cdot \nabla_y U \in L^2(Y)\}$. It is easy to see that U is a minimizer of $F(U)$ if and only if $a \cdot \nabla_y U = 0$.

The variation of $F(U)$ is

$$\frac{\delta F(U)}{\delta U}(V) = \int_Y (a \cdot \nabla_y U)(a \cdot \nabla_y V)\mathrm{d}y = -\int_Y a \cdot \nabla_y (a \cdot \nabla_y U) V \,\mathrm{d}y$$
$$= -\int_Y \nabla_y \cdot (aa^{\mathrm{T}} \nabla_y U) V \,\mathrm{d}y, \quad \text{for } V \text{ periodic in } y,$$

where we have used the incompressibility condition (2.1). aa^{T} is a 2×2 semi-positive definite matrix with rank 1.

To minimize the energy functional $F(U)$, we use a relaxation method, i.e. we solve the relaxed problem

$$\frac{\mathrm{d}U_\delta}{\mathrm{d}t} = -\frac{1}{\delta}\frac{\delta F(U_\delta)}{\delta U_\delta}$$

in order to reach an equilibrium state. Overall, the penalty scheme can be formulated as: find $U_\delta(x,y,t)$, such that

$$\begin{aligned} &\partial_t U_\delta + \nabla_x \cdot (a(x,y)U_\delta) = -\frac{1}{\delta}\frac{\delta F(U)}{\delta U} = \frac{1}{\delta}\nabla_y(aa^{\mathrm{T}}\nabla_y U_\delta), \\ &U_\delta(x,y,0) = U_0(x,y), \end{aligned} \tag{3.1}$$

where δ is the penalty parameter.

Remark 1. With the penalty term $\nabla_y(aa^{\mathrm{T}}\nabla_y U_\delta) = a \cdot \nabla_y(a \cdot \nabla_y U_\delta)$ in (3.1), we have

$$\partial_t U_\delta + \nabla_x \cdot (a(x,y)U_\delta) \in \mathscr{H}^\perp,$$

since for any periodic function $q(y) \in L^2(Y)$, by integration by parts,

$$\int_Y (a \cdot \nabla_y q)\varphi(y)\mathrm{d}y = \int_Y q(y)\nabla_y \cdot (a\varphi)\mathrm{d}y = 0 \quad \forall \varphi \in \mathscr{H},$$

i.e. $a \cdot \nabla_y q \in \mathscr{H}^\perp$.

Remark 2. The solution of the penalty equation (3.1) will convergence to that of the original homogenized equation (2.5) with the same initial condition when $\delta \to 0$.

To solve the penalty problem (3.1) efficiently, we use the operator splitting method.

Algorithm 1. At each time step t^n, given U^n:

- *Step 1*. For any $y \in Y = [0,1]^2$, find $U^*(x,y) = U(x,y,t^{n+1})$ by

$$\begin{aligned} &U_t + \nabla_x \cdot (aU) = 0, \quad x \in \Omega \subset \mathbb{R}^2, \\ &U(x,y,t^n) = U^n(x,y), \end{aligned} \tag{3.2}$$

  with prescribed boundary condition on the inflow part of the boundary.
- *Step 2*. For any $x \in \Omega$, solve the following problem in (t^n, t^{n+1}):

$$\begin{aligned} &U_t - \frac{1}{\delta}\nabla_y(aa^{\mathrm{T}}\nabla_y U) = 0, \quad y \in Y, \\ &U(x,y,t^n) = U^*(x,y), \end{aligned} \tag{3.3}$$

  subject to periodic boundary condition. Then set $U^{n+1} = U(x,y,t^{n+1})$.

The time step $\Delta t = t^{n+1} - t^n$ is determined by the CFL restriction (e.g. the CFL number is less than 1) when (3.2) is solved on a macro spatial grid for any fixed $y \in Y$. To solve (3.3) in Step 2, the same time step Δt is employed. Implicit scheme may be used in this step in order to make sure of the numerical stability.

3.2. The projection method

The homogenized equation (2.6) has the same structure as the incompressible Navier–Stokes equation

$$\begin{aligned} &\mathbf{u} \in H = \{\mathbf{u} \in (L^2(\Omega))^2 : \operatorname{div}\mathbf{u} = 0\}, \\ &\mathbf{u}_t + (\mathbf{u} \cdot \nabla)\mathbf{u} - \mu\Delta\mathbf{u} = -\nabla p \in H^\perp. \end{aligned}$$

This motivates us to design a projection method along the line of Chorin's work [2]. The general strategy is as follows:

Algorithm 2. At each time step, given $\{U^n\}$, we proceed in two steps:

- *Step 1*. Advance U^n to U^* by solving

$$\begin{aligned} &U_t + \nabla_x \cdot (aU) = 0, \\ &U(x, y, t^n) = U^n(x, y), \end{aligned} \tag{3.4}$$

  and let

$$U^*(x, y) = U(x, y, t^{n+1}).$$

- *Step 2*. U^{n+1} is set to be the projection of U^* onto $\mathscr{H}$ in the sense of L^2.

The projection operator amounts to averaging over ergodic components of the dynamical system associated with a on a torus $\mathbb{T}^2$. The efficiency of this algorithm hinges on whether this can be realized efficiently. So far we have only succeeded in finding efficient approximations to the projection operator for special flows fields. However, note that for both methods, the first steps of (3.2) and (3.4) are the same. The second step of the penalty method (3.3) can be regarded as an approximate projection. In the following, we will focus our discussion on penalty methods.

4. Numerical results

In this section, we present some numerical results for the penalty method. The results show that, by introducing the new independent variable y, we not only avoid treating the nonlocal and memory effect, but also capture some details in the microstructures, which is impossible with previous methods that only consider the macro homogenized equation for $U(x, t)$.

In these computations, the time step is adaptively defined by the CFL restriction that the CFL number is less than 0.8.

4.1. Shear flow

Consider the following problem:

$$\begin{aligned} &\partial_t u_\varepsilon + a\left(\frac{x_2}{\varepsilon}\right)\partial_{x_1} u_\varepsilon = 0, \quad x \in (-\infty, \infty) \times (0, 1), \ \ t \in (0, T), \\ &u_\varepsilon(x_1, x_2, 0) = u_0(x_1, x_2), \end{aligned} \tag{4.1}$$

with velocity $a = a(y_2) = 1 + \sin(2\pi y_2)$ and the initial data

$$u_0(x_1, x_2) = \begin{cases} 1.0 & \text{if } x_1 < 0, \\ 0.2 & \text{if } x_1 \geqslant 0. \end{cases}$$

Terminal time is set at $T = 0.3$. For $t \leqslant T$, we can reformulate this problem on a bounded domain $\Omega = (0,1) \times (0,1)$

$$\begin{aligned} &\partial_t u_\varepsilon + a\left(\frac{x_2}{\varepsilon}\right)\partial_{x_1} u_\varepsilon = 0, \quad (x, t) \in \Omega \times (0, T), \\ &u_\varepsilon(0, x_2, t) = 1.0, \quad x_2 \in (0, 1), t \in (0, T), \\ &u_\varepsilon(x_1, x_2, 0) = 0.2, \quad x \in \Omega. \end{aligned}$$

We solve the corresponding penalty equation (3.1) for $(x, y, t) \in (0, 1)^2 \times (0, 1)^2 \times (0, T)$ by Algorithm 1 with the penalty parameter $\delta = 0.1$.

To see the effectiveness of the penalty method, we first look at the maximum energy defined as $\max_{x\in\Omega}\int_Y |a\cdot\nabla_y U_\delta|^2 \mathrm{d}y$. We see in Table 1 that the energy is so small that we can neglect the penalty term in the penalty equation (3.1). This means that we actually solved the homogenized equation for shear flow (2.7)

$$\partial_t U + a(y_2)\partial_{x_1} U = 0.$$

By the method of characteristics, we have $U(x,y,t) = U_0(x_1 - a(y_2)t, x_2)$. If we replace y by x/ε, we get the exact solution for the shear flow (4.1).

Macro behavior. In Fig. 2, we present the result for $U(x,t) = (1/|Y|)\int_Y U_\delta(x,y,t)\mathrm{d}y$. It is apparent that the macro solution U displays diffusive behavior.

Local microstructure. Our method also captures the local microstructure at macro grid points. One example of such local microstructure is shown in Fig. 3.

Convergence as $h \to 0$. The fine scale solution to this problem is $u_\varepsilon = u_0(x_1 - a(x_2/\varepsilon)t, x_2)$. To obtain the exact macroscale solution, we average u_ε over the macro grid cell. The error between this exact macroscale solution and the computed solution $U(x,t) = (1/|Y|)\int_Y U_\delta(x,y,t)\mathrm{d}y$ by Algorithm 1 is displayed in Table 2. We see that the error converges to zero, but with fractional order of accuracy.

4.2. Flow with channels and islands

Consider the case when the stream-function is selected as

Table 1
Maximum energy at different time steps

Time	Maximum energy
0.1	1.11340120E − 7
0.2	1.13339647E − 7
0.3	1.13354346E − 7

Maximum energy is defined by $\max_{x\in\Omega}\int_Y |a\cdot\nabla_y U_\delta|^2 \mathrm{d}y$. Macro partition: $NX1 = NX2 = 20$; micro partition: $NY1 = NY2 = 12$; penalty parameter $\delta = 0.1$.

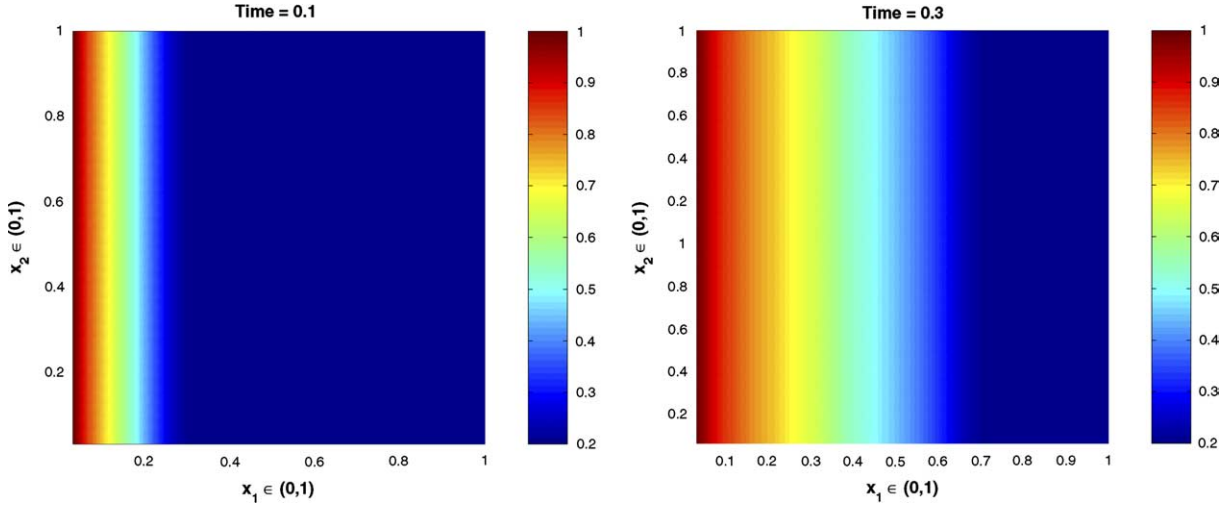

Fig. 2. Macro solution $U(x,t)$ at time = 0.1 (left); time = 0.3 (right). The macro grid is specified by $NX1 = NX2 = 32$. At each macro grid, we resolve the local cell Y with a $NY1 = NY2 = 16$ micro grid. Penalty parameter $\delta = 0.1$.

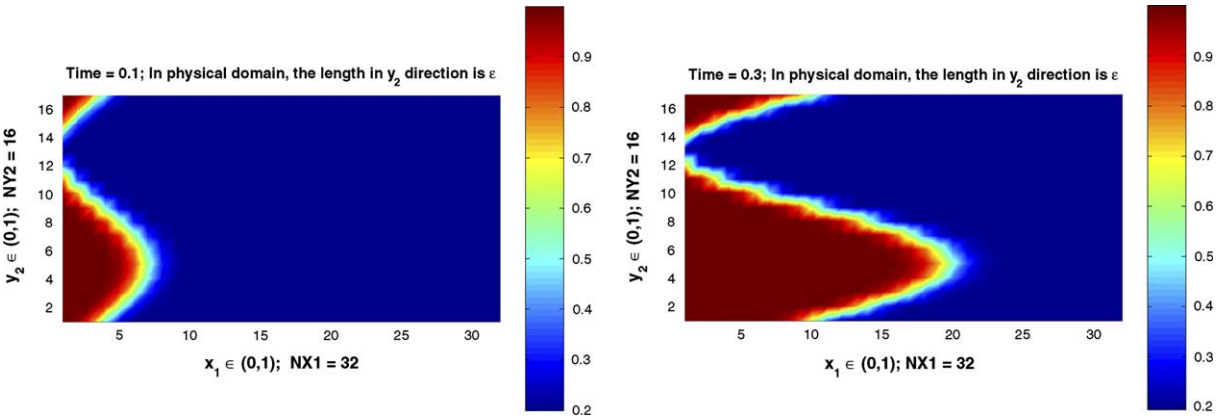

Fig. 3. The local microstructure behavior at the macro grid point $x_2 = 0$, at different x_1. The microstructure is independent of y_1. Therefore we only plotted the y_2-dependence over the cell of size ε. Penalty parameter $\delta = 0.1$. Time = 0.1 (left); time = 0.3 (right).

Table 2
Convergence in macro scale of the shear flow as $h \to 0$

Macro $NX1 \times NX2$	Micro $NY1 \times NY2$	Relative L^2 error
8×8	8×8	0.067799
16×16	16×16	0.045652
32×32	16×16	0.034779

Time = 0.3; $\varepsilon = 1/128$; penalty parameter $\delta = 0.05$.

$$\varphi(y) = \sin(2\pi y_1)\sin(2\pi y_2)/(4\pi) - \frac{y_2}{5}, \tag{4.2}$$

i.e.

$$a_1(y) = 0.2 - \sin(2\pi y_1)\cos(2\pi y_2)/2, a_2(y) = \cos(2\pi y_1)\sin(2\pi y_2)/2. \tag{4.3}$$

The streamlines are shown in Fig. 4. We can see that in each cell, there are 4 islands separated by some channels. The initial data $u_0(x)$ is chosen as

$$u_0(x) = \begin{cases} 0.2 & \text{if } x \in [1/4, 3/4] \times [1/4, 3/4], \\ 1.0 & \text{otherwise.} \end{cases}$$

On a finite time interval we may replace the original problem by

$$\begin{aligned} &\partial_t u_\varepsilon + \nabla \cdot (a(x/\varepsilon)u_\varepsilon) = 0 \quad \text{in } \Omega = (0,1)^2, \\ &u_\varepsilon|_{\partial\Omega} = 1.0, \\ &u(x,0) = u_0(x). \end{aligned}$$

The whole domain $[0,1]^2$ is divided into a uniform 16×16 grid. At each macro grid point, we resolve the fine scale details by a 32×32 grid over the square local micro cell $Y = [0,1]^2$, which is of size ε in physical domain.

As before, we first look at the effectiveness of penalty operator. In Table 3, we show the $\max_x \int_Y |a \cdot \nabla_y U_\delta(x,y)|^2 \, dy$ for different δ at time $t = 0.3$.

It is obvious that the convergence rate is of first order. Note that the penalty term in the penalty equation (3.1) only acts as streamline diffusion. But as a result of discretization, numerical cross-stream diffusion is

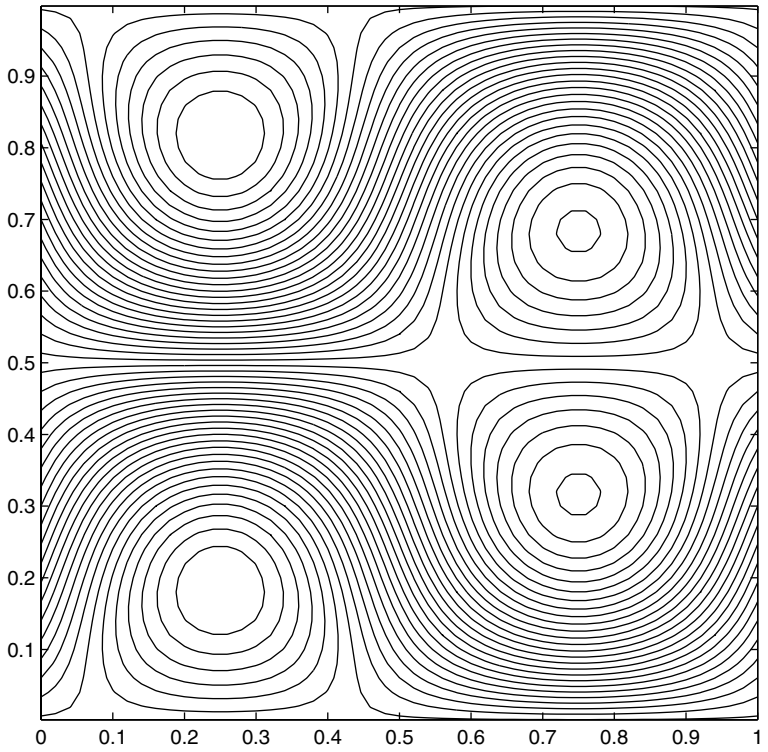

Fig. 4. Streamlines in a cell (one period).

Table 3
Energy convergence as $\delta \to 0$

δ	$\max_x \int_Y \lvert a \cdot \nabla_y U_\delta(x,y,t)\rvert^2 \mathrm{d}y$
0.4	0.0324507998
0.2	0.0139849046
0.1	0.0075101523
0.05	0.0036522540

Time = 0.3.

introduced. This diffusion effect increases as the penalty parameter δ decreases. Therefore in choosing δ, one has to consider the balance between effectiveness of averaging over the stream line and cross-stream diffusion.

Local microstructure. In Fig. 5, we plot the microstructure at the macro grid point $(x_1, x_2) = (\frac{5}{16}, \frac{1}{2})$. The effect of islands and channels is apparent.

Macro behavior. In Fig. 6, we show the result on $U(x,t) = (1/|Y|)\int_Y U_\delta \mathrm{d}y$.

Convergence as $h \to 0$. For $\varepsilon = 0.02$, we solve the original problem on fine grid 1024×1024 to obtain the 'exact' solution. We then average the fine scale exact solution over the macro cell to obtain the macroscale exact solution. In Table 4, we present the result of the convergence study of the error between the macro average of the 'exact' solution and the macro solution $U(x,t) = (1/|Y|)\int_Y U_\delta(x,y,t)\mathrm{d}y$ by Algorithm 1.

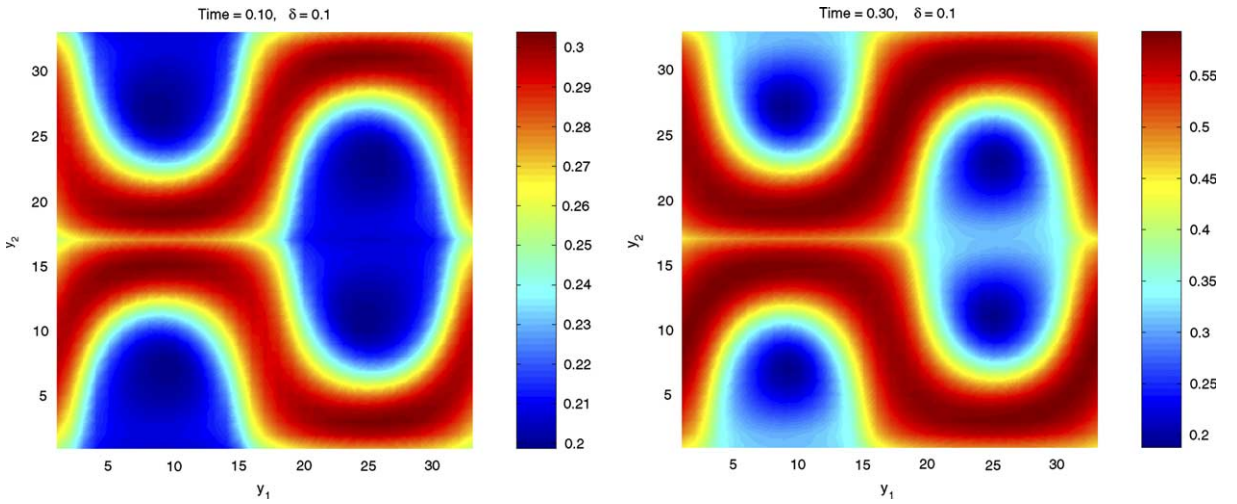

Fig. 5. Details inside the micro cell at $(x_1, x_2) = (5/16, 1/2)$, $\delta = 0.1$. Left: time $= 0.1$; Right: time $= 0.3$. The darker color regions are occupied by the islands and the lighter color regions are occupied by the channels.

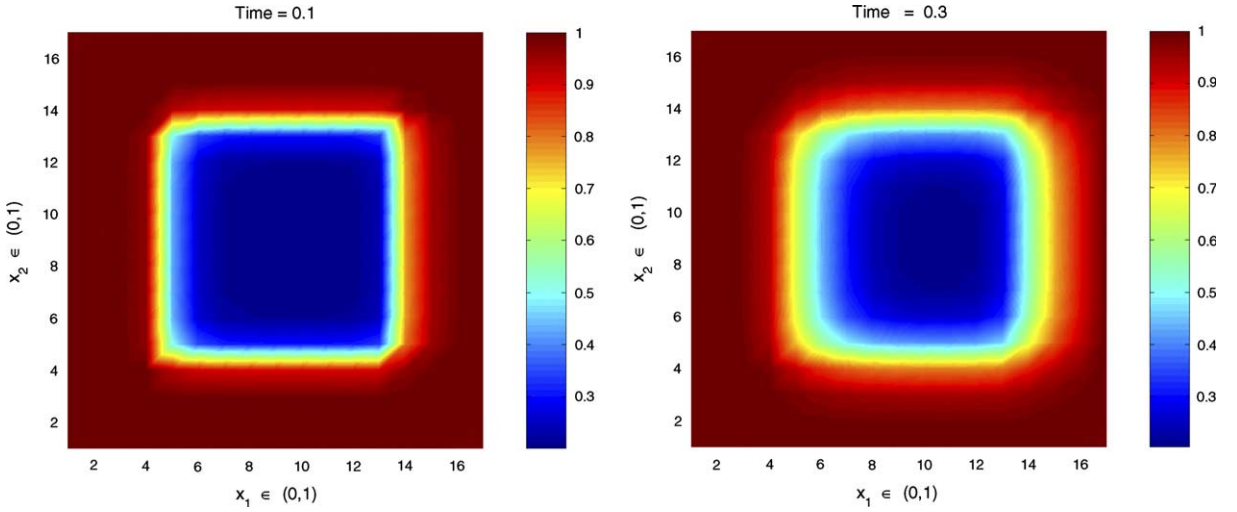

Fig. 6. Macro behavior of the flow with islands and channels at time $= 0.1$ (left), time $= 0.3$ (right); $\delta = 0.1$; macro grid: $NX1 = NX2 = 16$; micro grid: $NY1 = NY2 = 32$.

Table 4
Error in the macro scale solution when the macro and micro grids are refined

Macro $NX1 \times NX2$	Micro $NY1 \times NY2$	Relative L^2 error
8×8	8×8	0.120962
16×16	16×16	0.085031
32×32	32×32	0.073206

Time $= 0.3$, $\varepsilon = 0.02$, $\delta = 0.05$.

5. Extensions

It is important to note that the methodology developed here is much more general than solving linear transport equations with velocity fields that have periodic microstructures. We will discuss extension in two particularly interesting directions.

5.1. Nonlinear flux functions

We first consider the nonlinear transport problem.

$$\begin{aligned} &\partial_t u_\varepsilon + \nabla \cdot \left(a\left(x, \frac{x}{\varepsilon}\right) f(u_\varepsilon) \right) = 0, \quad x \in \mathbb{R}^2, \ \ t \in \mathbb{R}^+, \\ &u_\varepsilon(x,0) = u_0(x), \quad x \in \mathbb{R}^2, \end{aligned} \tag{5.1}$$

where the velocity field $a_\varepsilon = a(x, \frac{x}{\varepsilon})$ satisfies (2.1). The extension to nonlinear flux functions is quite straightforward. The homogenized equation takes the form [4]

$$\nabla_y \cdot (af(U)) = 0, \quad U_t + \nabla_x \cdot (af(U)) \in \mathscr{H}^\perp. \tag{5.2}$$

Note that the space $\mathscr{H}$ remains the same as before, and the first equation means that the flux $f(U)$ is constant along the streamlines. So it is sufficient to assume that the unknown U is constant along the streamlines, $\nabla_y \cdot (a(y)U) = a(y) \cdot \nabla_y U = 0$, i.e. $U \in \mathscr{H}$. Therefore, we can reformulate the homogenized equation (5.2) as

$$U(x,y,t) \in \mathscr{H}, \quad U_t + \nabla_x \cdot (af(U)) \in \mathscr{H}^\perp. \tag{5.3}$$

Similarly to the linear flux case, the penalty method can be used to solve this problem.

Algorithm 3. At each time step t^n, given U^n:

- *Step 1*. For any $y \in Y = [0,1]^2$, find $U^*(x,y) = U(x,y,t^{n+1})$ by

$$\begin{aligned} &U_t + \nabla_x \cdot (af(U)) = 0, \quad x \in \Omega \subset \mathbb{R}^2, \\ &U(x,y,t^n) = U^n(x,y), \end{aligned} \tag{5.4}$$

  with prescribed boundary condition at the inflow part of the boundary.
- *Step 2*. For any $x \in \Omega$, solve the following problem in (t^n, t^{n+1}):

$$\begin{aligned} &U_t - \frac{1}{\delta} \nabla_y (aa^{\mathrm{T}} \nabla_y U) = 0, \quad y \in Y, \\ &U(x,y,t^n) = U^*(x,y), \end{aligned} \tag{5.5}$$

  subject to periodic boundary condition. Then set $U^{n+1} = U(x,y,t^{n+1})$.

In the following, we show a numerical example using this algorithm. We consider the problem (5.1) in a unit square $\Omega = [0,1]^2$ with the velocity field a and the flux $f(u)$ given by

$$\begin{aligned} &a = (a_1, a_2)^{\mathrm{T}}, \quad a_1(y) = a_1(y_1, y_2) = 1.1 - \cos(2\pi y_2), \ \ a_2 = 0, \\ &f(u) = \frac{u^2}{u^2 + (1-u)^2/M}, \end{aligned}$$

and subject to the following boundary and initial conditions:

Table 5
Convergence in macro scale of nonlinear transport equation as $h \to 0$

Macro $NX1 \times NX2$	Micro $NY1 \times NY2$	Relative L^2 error
8×8	8×8	0.092711
16×16	16×16	0.040398
32×32	16×16	0.028949

Time $= 0.6$, $M = 2$, $\varepsilon = 0.02$, $\delta = 0.05$.

$$u(x,0) = 0, \quad x \in \Omega,$$
$$u = 1 \quad \text{at left boundary } x_1 = 0.$$

In Table 5, we present the numerical results for the macroscale behavior of the solution. As before, to obtain the exact solution, we first compute the fine scale solution on a fine mesh, then average this fine scale solution over the macro cell to obtain the "exact" macroscale solution. The error between this "exact" macroscale solution and the computed macroscale solution is shown in Table 5.

5.2. Random velocity fields

Consider the case when $a^\varepsilon(x) = a(x, \frac{x}{\varepsilon})$, and $a(x,y)$ is a random stationary process in y, for each fixed x. $\varepsilon = (\varepsilon_1, \varepsilon_2)$ is the correlation length in the x_1, x_2 directions respectively. In this case we can approximate $a(x,y)$ by periodic functions in y with sufficiently large periods that capture the essential statistics of a. This was done in [14] for the pressure equation in porous media (elliptic homogenization problem). The same principle can be adopted here (see Fig. 1). The basic philosophy is to probe at each macro grid point the local microstructure, instead of just the function values at that grid point. If the local microstructure is periodic, the size of the local cells may be exactly equal to that of a period. Otherwise the size of the local cells is a few times of the local correlation length of the microstructure.

Denote by Ω_c the set of the macro grid point, and still by Y the set of the micro grid point of the local cell. (Note that Y is the actual local computational micro cell now, not the unit square in periodic case considered earlier.) We propose the following numerical procedure:

Algorithm 4. At each time step t^n, given U^n:

- *Step 1.* For any $y \in Y$, find $U^*(x,y) = U(x,y,t^{n+1})$ by solving the following problem on the macro mesh with mesh points Ω_c:

$$\begin{aligned} &U_t + \nabla_x \cdot (af(U)) = 0, \\ &U(x,y,t^n) = U^n(x,y), \end{aligned} \tag{5.6}$$

  with prescribed boundary condition at the inflow part of the boundary.
- *Step 2.* For any $x \in \Omega_c$, solve the following problem in (t^n, t^{n+1}) on the micro grid with grid points Y

$$\begin{aligned} &U_t - \frac{1}{\delta} \nabla_y \cdot \left(aa^{\mathrm{T}} \nabla_y U \right) = 0, \\ &U(x,y,t^n) = U^*(x,y), \end{aligned} \tag{5.7}$$

  subject to periodic boundary condition. Then set $U^{n+1} = U(x,y,t^{n+1})$.

Remark. Even if we choose the micro cell Y to be the same size as the macro cell, the cost of this algorithm is much less than the fine grid method, because we can employ macro time steps in Step 1 rather than micro time steps in fine grid method.

To demonstrate the efficiency of this algorithm, we consider the problem (5.1) in a unit square $\Omega = [0,1]^2$ with a random velocity field a and the flux $f(u)$ given by

$$f(u) = \frac{u^2}{u^2 + (1-u)^2/M},$$

and subject to the following initial and boundary conditions:

$$u(x,0) = 0, \quad x \in \Omega,$$
$$u = 1 \quad \text{at } x_1 = 0.$$

The random velocity field a is given by Darcy's law $a = -K\nabla p$, where $K = K(x_1/\varepsilon_1, x_2/\varepsilon_2)$ is a stochastic log-normal permeability field (the normal field is mean-zero with variance σ^2 and correlation length $\varepsilon = (\varepsilon_1, \varepsilon_2)$) and the pressure p satisfies that

$$-\nabla \cdot (K\nabla p) = 0 \quad \text{in } \Omega \tag{5.8}$$

subject to the boundary conditions: $p = 1$ at the left boundary $x_1 = 0$; $p = 0$ at the right boundary $x_1 = 1$; the top and bottom boundaries are close to flow $\partial p/\partial n = 0$.

First we generate a realization of a log-normal permeability field K by the moving ellipse averaging method [19] on a 512×512 mesh (the normal field is mean-zero with variance $\sigma^2 = 1$ and correlation length $\varepsilon_1 = 0.08$, $\varepsilon_2 = 0.01$). Then we solve (5.8) on the 512×512 grid to obtain the velocity field a. Lastly we solve (5.1) with the prescribed initial and boundary conditions by Algorithm 4. In Fig. 7, the result is presented on the finest 512×512 grid. In Fig. 8, we present the result of Algorithm 4 on a coarse 32×32 grid with the local micro cell chosen to be the same size as the macro cell. It can be seen that some features of the solution are captured.

One can see that there is still appreciable amount of error in the numerical solutions computed by the multiscale method. In particular, the numerical solution gives an earlier first arrival time. This is mainly due to the lack of sufficient resolution at the small scales.

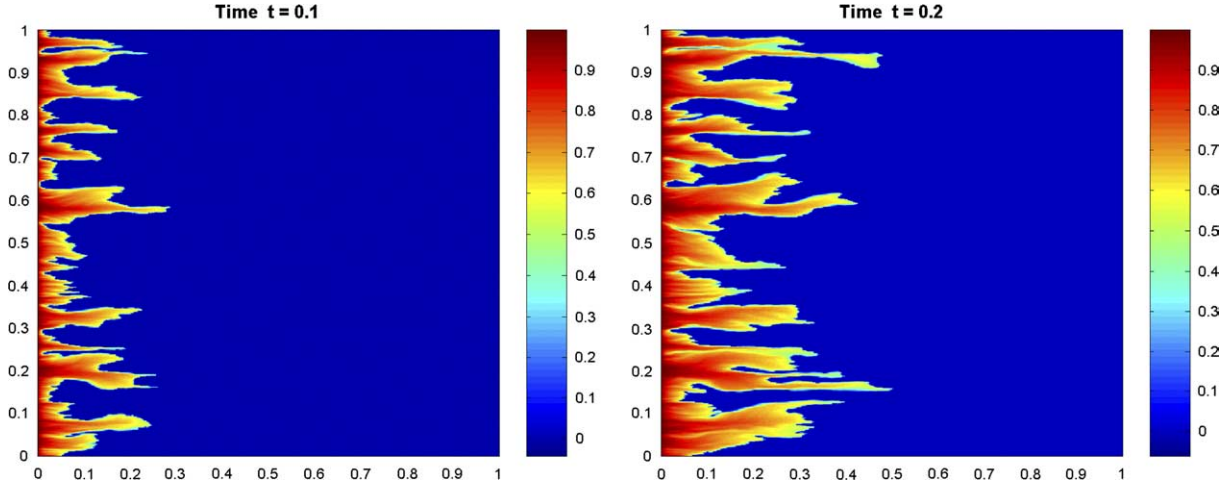

Fig. 7. Fine grid solution for problem with a typical realization of random velocity field. $\varepsilon = (0.08, 0.01)$, $\sigma = 1.0$, $M = 2$. (left) Time = 0.1; (right) time = 0.2.

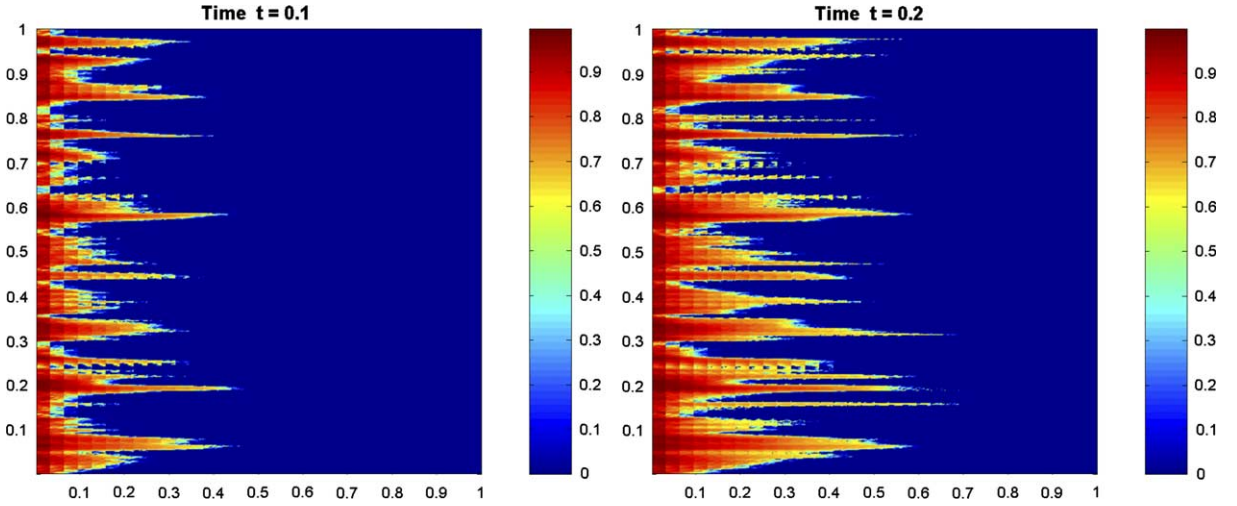

Fig. 8. Coarse grid solution for problem with a typical realization of random velocity field. $\varepsilon = (0.08, 0.01)$, $\sigma = 1.0$, $M = 2$, $\delta = 0.1$. (left) Time = 0.1; (right) time = 0.2.

6. Two-phase flow in porous media

We apply the algorithm developed in the previous section to two-phase flow in porous media, under the assumption that the displacement is dominated by viscous effects; i.e., we neglect the effects of gravity, compressibility, and capillary pressure. Porosity is taken to be constant. The two phases are referred to as being water and oil, designated by subscripts w and o, respectively (see [8]). Combining Darcy's law with the conservation of mass allows us to write the governing equations in terms of the so-called pressure and saturation equations:

$$\nabla \cdot (\lambda(s) K \nabla p) = 0, \tag{6.1}$$

$$\frac{\partial s}{\partial t} + \mathbf{v} \cdot \nabla f(s) = 0, \tag{6.2}$$

where s is the saturation of the water phase satisfying that $0 \leqslant s \leqslant 1$, p is the pressure, K is the absolute permeability of the porous media, λ is the total mobility, f is the fractional flow of water, and $\mathbf{v}$ is the total velocity:

$$\begin{aligned} \lambda(s) &= \frac{K_{rw}(s)}{\mu_w} + \frac{K_{ro}(s)}{\mu_o}, \\ f(s) &= \frac{K_{rw}/\mu_w}{K_{rw}/\mu_w + K_{ro}/\mu_o}, \\ \mathbf{v} &= \mathbf{v}_w + \mathbf{v}_o = -\lambda(s) K \nabla p. \end{aligned} \tag{6.3}$$

In the above, k_{rw}, k_{ro} are the relative permeability of water and oil phases, respectively; $\mathbf{v}_w = -(K_{rw}(s)K/\mu_w)\nabla p$ and $\mathbf{v}_o = -(K_{ro}(s)K/\mu_o)\nabla p$ are the velocity of water and oil phase given by Darcy's law. Due to the heterogeneity of the porous media, we assume the absolute permeability has the form $K = k(x, \frac{x}{\varepsilon})$, where ε is the local correlation length.

The pressure equation (6.1) can be upscaled in many ways, for example, using the heterogeneous multiscale method (HMM, [5]). The saturation equation, however, is a different story. We have seen in

the previous sections that even for the simplest case when the microstructure is locally periodic, the macroscale behavior of the solutions to the transport equation can be quite complicated, and in particular, depends on memory. Current upscaling procedures for the saturation equation used either moment averaging or volume averaging (see [3,8,9,12]). They are all a bit ad hoc at some level. Furthermore, the pressure equation (6.1) and the saturation equation (6.2) is coupled, the microstructure of the saturation is needed to upscale the pressure equation. Such information is absent with the moment or volume averaging methods discussed earlier. However, the procedure proposed here does yield some microscale information, which makes it possible to upscale the whole system.

Algorithm 5. At each time step t^n, given $S^n(x,y)$:

- *Step 1.* Upscale the pressure equation (6.1) to obtain $P^n(x)$ (by HMM-finite volume method), and retrieve the microscale velocity v^n (6.3) at the place needed (refer to Fig. 1), by the periodic extension method for the periodic case [5,7] or by a post-processing procedure for the random case [16,14].
- *Step 2.* Upscale the saturation equation (6.2) to obtain $S^{n+1}(x,y)$ by Algorithm 3 for the periodic case and by Algorithm 4 for the random case.

Remark. Heterogeneous multiscale method (HMM, [5]) has two main components:

- Selecting the macroscale solver (we choose the finite volume method).
- Estimating the needed data for implementing the selected macroscale solver, using the microscale model (an implementation for elliptic homogenized problems can be found in [14]).

In the following, we present some numerical results. The domain of the porous media is taken to be the unit square. In all cases, we fix pressure and saturation ($s = 1$) at the inlet edge (left: $x_1 = 0$) and we also fix the pressure (less then that at inlet edge) at the outlet edge (right: $x_2 = 1.0$). The top and bottom edges are closed to flow. We set the relative permeability of oil and water to be simple quadratic functions of their respective saturations; i.e.,

$$K_{rw} = s^2, \quad K_{ro} = (1-s)^2.$$

Let M be the ratio of oil and water viscosity ($M = \mu_o/\mu_w$). Results are presented in terms of *oilcut* (i.e., the fraction of oil in the produced fluid q_o/q_t, with q_o being the volumetric flow rate of oil produced at the outlet edge and q_t being the volumetric flow rate of total fluid produced at the outlet) versus pore volumes injected (PVI). PVI is analogous to dimensionless time and is defined as $\int_0^t q_t(\tau)\mathrm{d}\tau/V_\mathrm{p}$, where t is dimensional time and V_p is the total pore volume in the whole media.

Periodic case. In this case, we assume the porous media is periodic. We set the absolute permeability to be

$$K\left(x,\frac{x}{\varepsilon}\right) = \frac{1.2+\sin(2\pi x_1/\varepsilon)}{1.2+\sin(2\pi x_2/\varepsilon)} + \frac{1.2+\sin(2\pi x_2/\varepsilon)}{1.2+\cos(2\pi x_1/\varepsilon)} + \sin(4(x_1^2+x_2^2)) + 1$$

with $\varepsilon = 1/64$. The result is depicted in Fig. 9. The solid curve was obtained by solving the two-phase system on a 512×512 grid, and the dash curve was obtained by Algorithm 5 on the coarse 16×16 mesh, with $M = 2$, $\delta = 0.05$.

Random cases. As an example of random media, the absolute permeability field $K = K(x, x_1/L_1, x_2/L_2)$ is taken to be a log-normal stochastic field, and the mean-zero normal filed is randomly generated with parameters: L_1, which is the correlation length in the x_1 direction and L_2, which is the correlation length in the x_2 direction. The variance is σ^2. We computed two examples: one for $L_1 = L_2 = 0.02, \sigma = 1.0$ and

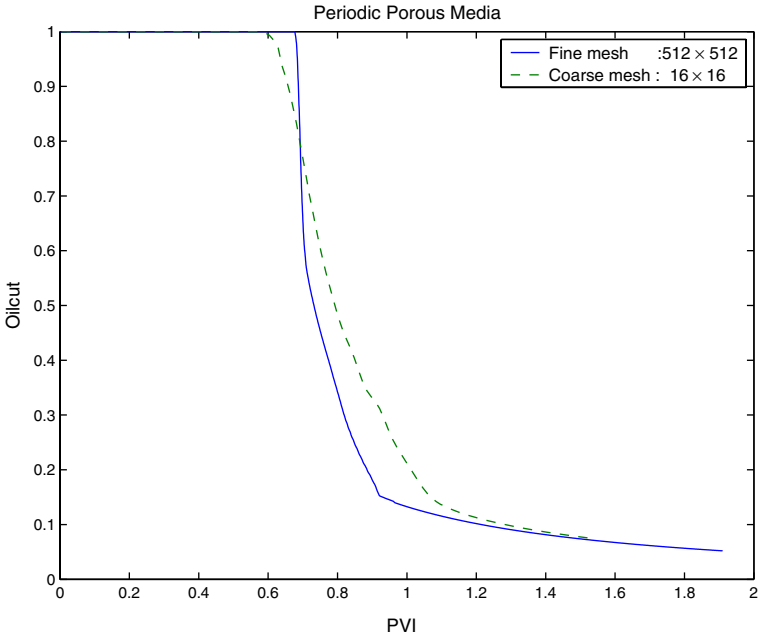

Fig. 9. Fractional flow of oil at outlet edge for the case of periodic media. $\varepsilon = 1/64$, $M = 2$, $\delta = 0.05$.

the other for $L_1 = 0.08, L_2 = 0.02, \sigma = 1.0$. The results were shown in Fig. 10 for two typical realizations of the log-normal absolute permeability field generated by the moving ellipse averaging method.

Comparing Figs. 9 and 10, we see that the numerical solution is much more accurate for the periodic case than for the random case. This is not a surprise, since in the random case, there is a phase error that contributes to the dynamics.

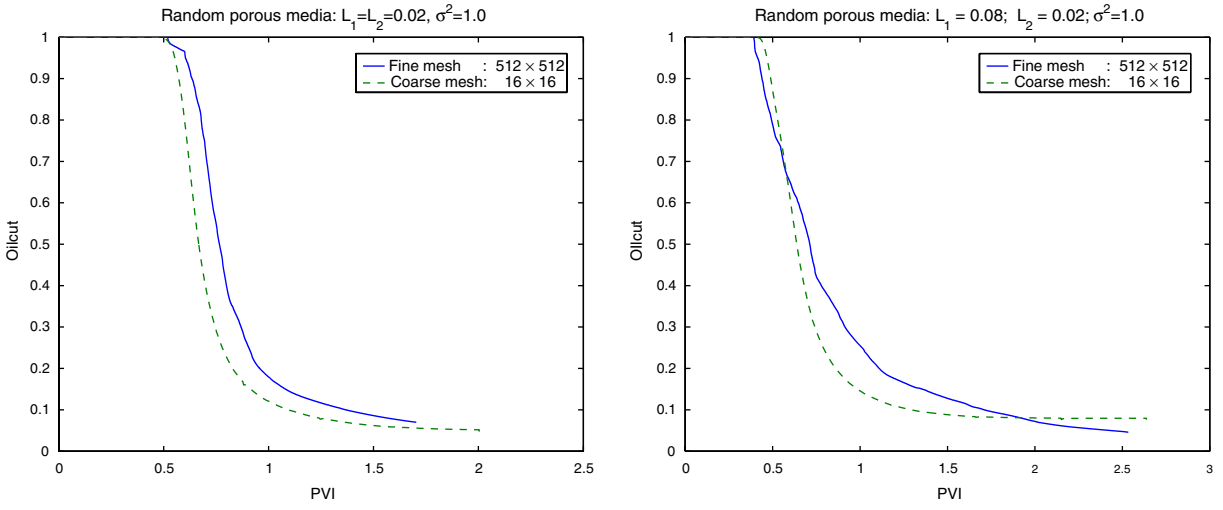

Fig. 10. Fractional flow of oil at outlet edge for random media for two typical realization of the absolute permeability with different statistics parameters. $M = 2$, $\delta = 0.05$. (left) $L_1 = L_2 = 0.02$, $\sigma = 1.0$; (right) $L_1 = 0.08$, $L_2 = 0.02$, $\sigma = 1.0$.

7. Conclusions

We have developed a method whose cost is independent of ε. The basic philosophy is to probe at each macro grid point the local microstructure, instead of simply the function values at that grid point. The local microstructure is encoded in the dependence on y, the new independent variable introduced.

We have found, as expected, that the numerical results are more accurate for the case of periodic microstructure than for the case of random microstructure. The reason is as follows. In the periodic case, the solutions have the so-called "two-scale regularity" [13], i.e. the microscale structure varies smoothly (pointwise) on the macroscale. In the random case, even though this is still true in a statistical sense, it is not true in the pointwise. Nevertheless, our evolution algorithm does make use of this smoothness in the pointwise sense, since we use interpolation to recovers values of the velocity field in the regions which are not represented by the grid shown in Fig. 1. Our next task is to extend the methodology presented here to capture the statistical behavior in the random case.

This methodology can be extended to other systems such as the Carleman equation [10,5] for which HMM does not work directly [5].

Acknowledgments

The authors thank the referees for their thorough reading the manuscript and very valuable comments. The work of E is supported in part by ONR Grant N00014-01-1-0674. The work of Yue is supported in part by NSF of China (10471102).

References

[1] G. Allaire, Homogenization and two-scale convergence, SIAM J. Math. Anal. 23 (1992) 1482–1518.
[2] A.J. Chorin, Numerical solution of the Navier–Stokes equations, Math. Comput. 22 (1968) 745–762.
[3] M.A. Christie, Upscaling for reservoir simulation, J. Petrol. Technol. 48 (1996) 1004–1010.
[4] W. E, Homogenization of linear and nonlinear transport equations, Commun. Pure Appl. Math. XLV (1992) 301–326.
[5] W. E, B. Engquist, The heterogeneous multi-scale methods, Commun. Math. Sci. 1 (2003) 87–120.
[6] W. E, B. Engquist, The heterogeneous multi-scale method for homogenization problems, Multiscale Model. Simulat., submitted. Available at <http://www.math.princeton.edu/multiscale/>.
[7] W. E, P.B. Ming, P.W. Zhang, Analysis of the heterogeneous multiscale method for elliptic homogenization problems, J. AMS 18 (2005) 121–156.
[8] Y. Efendiev, L.J. Durlofsky, Numerical modeling of subgrid heterogeneity in two phase flow simulations, Water Resour. Res. 38 (2002) 1128–1138.
[9] Y. Efendiev, L.J. Durlofsky, A generalized convection–diffusion model for subgrid transport in porous media, Multiscale Model. Simulat. 1 (2003) 504–526.
[10] B. Engquist, Computation of oscillatory solutions to hyperbolic differential equations, Springer Lect. Notes Math. 1270 (1987) 10–22.
[11] L.C. Evans, The perturbed test function method for viscosity solutions of nonlinear PDE, Proc. Roy. Soc. Edinburgh 111A (1989) 359–375.
[12] P. Langlo, M.S. Espedal, Macrodispersion for two-phase, immisible flow in porous media, Adv. Water Resour. 17 (1994) 297–316.
[13] A.-M. Matache, C. Schwab, Two-scale FEM for homogenization problems, Math. Model. Numer. Anal. 36 (2002) 537–572.
[14] P.B. Ming, X. Yue, Numerical methods for multiscale elliptic problems. Preprint 2003. Available at <http://www.math.princeton.edu/multiscale/>.
[15] G. Nguetseng, A general convergence result for a functional related to the theory of homogenization, SIAM J. Math. Anal. 20 (1989) 608–623.
[16] J.T. Oden, K.S. Vemaganti, Estimation of local modelling error and global-oriented adaptive modeling of heterogeneous materials: error estimates and adaptive algorithms, J. Comput. Phys. 164 (2000) 22–47.

[17] C. Schwab, A.-M. Matache, Generalized FEM for homogenization problems, in: T.J. Barth et al. (Eds.), Lecture Notes in Computational Science and Engineering, Springer, Berlin, 2002.
[18] L. Tartar, Solutions oscillantes des quations de Carleman, Goulaouic–Meyer–Schwartz Seminar, 1980–1981, Exp. No. XII, 15 pp., cole Polytech., Palaiseau, 1981.
[19] T.C. Wallstrom, S. Hou, M.A. Christie, L.J. Durlofsky, D.H. Sharp, Accurate scale up of two phase flow using renormalization and nonuniform coarsening, Comput. Geosci. 3 (1999) 69–87.
[20] D. Zhang, L. Li, H.A. Tchelepi, Stochastic formulation for uncertainty analysis of two-phase flow in heterogeneous reservoirs, SPE J. 5 (2000) 60–70.